RESEARCH PAPER

The suppression of solidification cracking of Al welds by regulating Zn/Mg ratio

Di Zhang [1,2] · Xin Zhao [1] · Yanlin Pan [1] · Hongxiang Li [1,2] · Li Zhou [3] · Jishan Zhang [1,2] · Linzhong Zhuang [1,2]

Abstract

7xxx series aluminum alloys are susceptible to solidification cracking during fusion welding. This study systematically investigates the solidification cracking susceptibility of T-$Mg_{32}(AlZn)_{49}$-strengthened Cu-free Al-Mg-Zn alloy with a Zn/Mg ratio below 1.0. The alloy is different from η-$MgZn_2$-strengthened 7xxx series alloys whose Zn/Mg ratios are above 1.0. The crack length of the studied Al-Mg-Zn series alloys is shorter than traditional Cu-free 7xxx series alloys, which corresponds to lower solidification cracking tendency. Welding cracks tend to grow along the continuous eutectic phases during the end of welding solidification, and thus, cracks occur when liquid can no longer hold the constraining stress. According to the results, Al-Mg-Zn series alloys have the narrower eutectic temperature range and narrower mushy zone than 7xxx series alloys. Thus, the constraining stress during solidification is lower than 7xxx series alloys. The liquid fractions of the Al-Mg-Zn series alloys are relatively high than 7xxx series alloys, making it possible to heal micro-cracks during the end of solidification process.

Keywords Al alloy · Welding · Solidification cracking susceptibility · Microstructure evolution · Non-equilibrium solidification

1 Introduction

7xxx series aluminum alloys are extensively used in aerospace, shipbuilding, and vehicle industry mainly because of their high strength to weight ratio, fracture toughness, and larger damage tolerance [1, 2]. However, Liptak [3] showed that the Al alloy was susceptible to solidification cracking when the alloy contains 1 to 4% Mg, 0 to 5% Cu, or 4 to 9% Zn. These high strength alloys were proven to be susceptible to solidification cracking during direct chill casting or

fusion welding. On the other hand, 5xxx series aluminum alloys has medium strength, good corrosion resistance, and good weldability [4, 5]. Thus, one of the urgent problems is how to suppress the weld solidification cracking while simultaneously maintaining the strength of the Al alloy. Generally, solidification cracks usually take place at the ending period of the welding solidification process, during which time solid phases occur as temperature cooling down, and grains begin to contact with their neighboring ones. When this happens, a rigid network of dendritic grains is formed, and the unsolid liquid could not move freely. These thin liquid layers between grains are neither able to bear nor to transfer constraining stress during solidification, leading to cracks on alloys with lower weldability when welds cannot hold the constraining stress anymore.

An effective method to improve the weldability of the Al-Mg-Si alloy was by regulating prior thermal temper of the alloy. The hot cracking susceptibility during welding was high in the T6 temper as compared with T4 temper, which is related to the width of the partially melted zone [6]. It was presented that solidification cracking during welding could be eliminated in deep and narrow welds produced by laser welding [7]. However, the cost of laser welding was much higher than traditional tungsten-inert gas welding or metal inert gas welding. Kou studied the effect of magnetic arc oscillation

✉ Di Zhang
zhangdi@skl.ustb.edu.cn

1 State Key Laboratory of Advanced Metals and Materials, University of Science and Technology Beijing, Beijing 100083, People's Republic of China

2 Beijing Laboratory of Metallic Materials and Processing for Modern Transportation, University of Science and Technology Beijing, Beijing 100083, People's Republic of China

3 Shandong Provincial Key Laboratory of Special Welding, Harbin Institute of Technology at Weihai, Weihai 264209, People's Republic of China

Table 1 Experimental alloy composition in wt.% (balance: Al)

|	Mg	Zn	Cu	Cr	Ti	Zr	Fe	Si	Zn/Mg
Alloy0	5.0	0	0.15	0.03	0.07	0.15	0.20	0.15	0
Alloy1	5.0	1.0	0.15	0.03	0.07	0.15	0.20	0.15	0.2
Alloy2	5.0	2.0	0.15	0.03	0.07	0.15	0.20	0.15	0.4
Alloy3	5.0	3.0	0.15	0.03	0.07	0.15	0.20	0.15	0.6
AlloyC	3.0	4.0	0.05	0.2	0.07	0.15	0.15	0.15	1.3

on the grain structure and solidification cracking of aluminum alloy welds [8]. Transverse arc oscillation at low frequencies could produce alternating grain orientation and this type of grain structure was effective in reducing solidification cracking. Research showed that pulsed electric current could refine the grain structure of aluminum alloys [9] and suppress the hot cracking of Al alloys. Similarly, the crack in the 1045 steel could be healed by electro-pulsing treatment [10]. Although arc oscillation and pulsed electric current were effective on suppressing the weld hot cracking, they were expensive and still difficult to apply in the real industry.

During the last decade, microalloying elements, such as Sc [11, 12], Er [13], and Ag [14, 15], in the base metal or filler metals were usually used to improve the weldability of high strength Al alloy. It showed that the reduction of hot cracking susceptibility was due to the reduction of solute segregation, rise of solidification temperature, and refined grains. Moreover, by adding such alloying elements, the strength of the alloy can be improved by dispersion strengthening, precipitation strengthening, and grain refinement [16–18]. However, compared with traditional 7xxx series aluminum alloys, the cost of Sc, Er, and Ag limits the development of such alloys and is not infeasible for industrial applications. In addition, Janaki [19] investigated the use of inoculants on the grain refinement and weldability of AA2090 Al alloys. It proved that Zr was the most useful

inoculants than Ti and Ti-B to improve the weldability of the Al alloys. The strength of the alloy was only about 20 MPa higher than the alloys without inoculants.

Various studies have demonstrated that solidification cracking susceptibility has been influenced by several metallurgical factors. DuPont [20] concluded that the wider the solidification temperature range and eutectic region in the weld metal, and thus the larger the susceptible to solidification cracking during fusion welding. The amount of liquid during terminal solidification was another important factor for the occurrence of solidification cracking. The abundant enough eutectic liquid between grains can suppress and heal the initial cracks. Beneficial eutectic reactions can also impede the crack propagation throughout the mushy zone by changing the liquid distribution along the grain boundary [21]. Kou S [22] has proposed a simple test for assessing solidification cracking susceptibility and checked its validity on solidification susceptibility. Such metallurgical factors were proven to be effective on the cracking susceptibility of superalloy or steel.

The chemical composition of the aluminum alloy has a great influence on the eutectic reaction, amount and distribution of liquid during terminal stage of solidification, and thus dramatically alters the solidification cracking tendency of the Al alloy. In our previous study, Zn-modified 5xxx series aluminum alloys with Zn/Mg ratio below 1.0 have been developed with higher mechanical strength to meet the requirement of marine and vehicle users and to provide theoretical and experimental basis for engineering design and application of novel alloys [23]. The age hardening precipitates in the novel Al-Mg-Zn alloy is T-$Mg_{32}(AlZn)_{49}$ phase [24, 25], which is different from the commonly known η-$MgZn_2$ phase in 7xxx series aluminum alloys (Zn/Mg > 1.0). However, the solidification cracking behavior during fusion welding of the novel alloy has not been investigated. Thus, in this study, Houldcroft fishbone test is applied to determine the solidification cracking susceptibility during fusion welding of the novel Al-Mg-Zn

Fig. 1 Top view of the fishbone specimen [3]
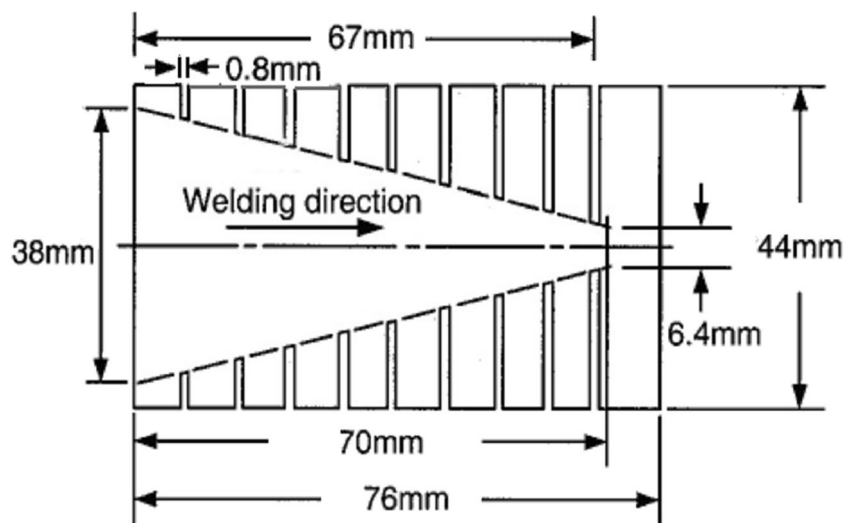
Fig. 2 **a** Engineering stress-strain curves and **b** mechanical properties of the alloys
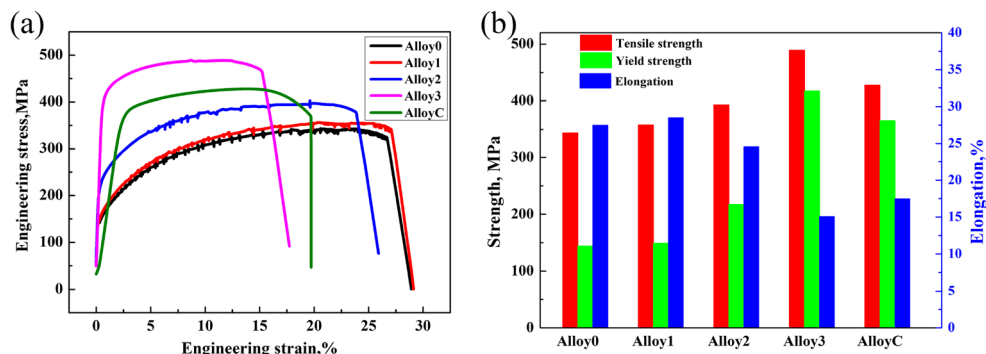
series alloys. The microstructures are observed by optical microscopy and scanning electron microscopy (SEM). Non-equilibrium solidification behavior of all alloys is calculated to find out the solidification features and the liquid distribution patterns during welding processes. Both these simulations are used to make explanations and even predictions for solidification cracking tendency during welding.

2 Materials and methods

2.1 Materials and tensile testing

In this study, four Al-Mg-Zn alloys with different Zn contents were investigated, with a Cu-free 7xxx series alloy (AA7039) as a contrast alloy (AlloyC). The composition of all alloys is listed in Table 1. The Zn/Mg ratio of the novel alloy is below 1.0 compared with traditional 7xxx series alloy where Zn/Mg ratio usually above 1.0. All alloys were melted, homogenized, hot and cold rolled to a final thickness of 2.5 mm. Then, the alloys were solution treated and artificially aged at 90 °C for 24 h and subsequently aged at 140 °C for another 24 h.

The tensile test specimens were taken in the rolling direction with a gauge length of 25 mm and width of 6 mm followed by ASTM E8 standards. The tensile properties of aged specimens were tested at room temperature with an initial strain rate of 4.8×10^{-4} s^{-1}. Each reported tensile testing value was the average of three individual tests.
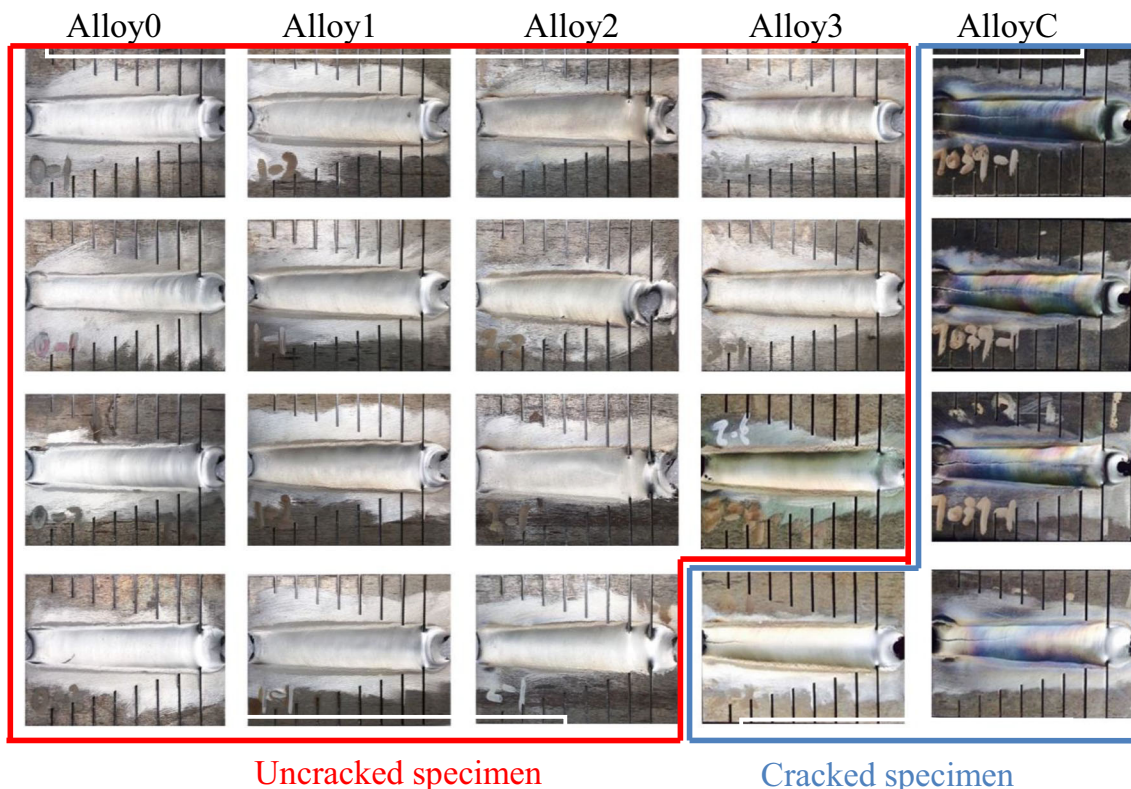
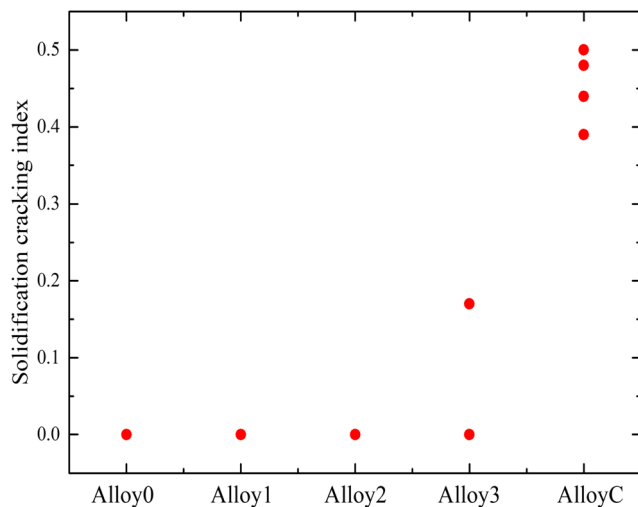Fig. 3 Representative pictures of cracked and uncracked welds

Fig. 4 Welding solidification cracking index of all alloys

2.2 Weldability evaluations

Houldcroft fishbone test is used for evaluating the solidification cracking tendency during welding process [3]. All fishbone test specimens with a thickness of 2.5 mm are machined from the alloys as depicted in Fig. 1. A specimen with slots of varying depth is free from outside constraints during welding process. As welding starts from the starting edge of the specimen, initial crack occurs during solidification and propagates along its centerline. The welding solidification cracking index is defined as the crack length divided by the total length of the specimen and is used to estimate the solidification cracking susceptibility of different specimens.

Four parallel specimens were used to test the solidification cracking tendency of each alloy for the accuracy purpose. Tungsten-inert gas welding without filler metal was applied, since the solidification cracking susceptibility of base metal was the only consideration in this test. The welding processes were conducted by YASKA VA-HP20D PLC-controlled manipulator equipped with INVERTIG PRO digital 240 AC/DC welding system. The electrode type was tungsten and the angle was 90°. The welding current and welding speed were 130 A and 4 mm/s, respectively, with an Ar shielding flow rate of 15 L/min. The arc length and arc voltage were 4 mm and 12 V, respectively.

2.3 Microstructure observation and simulation

The microstructure of the welds was examined by SEM. Energy-dispersive spectrum (EDS) was applied to analyze the chemical composition of the eutectic phases in the welds. For those uncracked specimens, direction paralleled to welding direction (direction A) was chosen to observe the microstructure of welds. For those cracked specimens, apart from the previous direction, surface perpendicular direction (direction B) was also selected to examine the microstructure of welds. The number and size of the micro-cracks on all welds were measured by an image processing software. Non-equilibrium solidification behavior of all alloys during welding process was calculated by FactSage software.

3 Results

3.1 Mechanical properties

The engineering stress-strain curves and mechanical properties of the studied alloys are shown in Fig. 2. The results show that both the tensile and yield strengths increase gradually with an increase of Zn/Mg ratio (Zn/Mg ≤ 1), while the elongation decreases. With further increase of Zn/Mg ratio, the strength of the alloy begins to decrease. The tensile strength of novel Alloy3 can be up to 490 MPa, which is higher than that of AlloyC. It means that the novel alloy has the same strength level compared with the Cu-free 7000 series alloys.

3.2 Solidification cracking tendency during welding

The solidification cracking susceptibility of all tested specimens is shown in Fig. 3. Continuous cracks are observed in all AlloyC specimens and one out of four Alloy3 specimens. All 12 Alloy0, Alloy1, Alloy2 specimens show no visible cracks and similar levels of weldability. Figure 4 shows the welding solidification cracking index of all the alloys. AlloyC specimens have the highest solidification cracking susceptibility among all tested alloys. The solidification cracking index of Alloy3 is lower than AlloyC, indicating its lower solidification cracking tendency compared with AlloyC. The
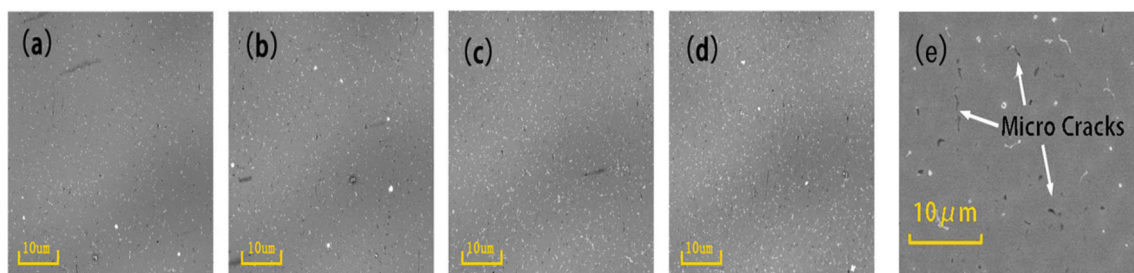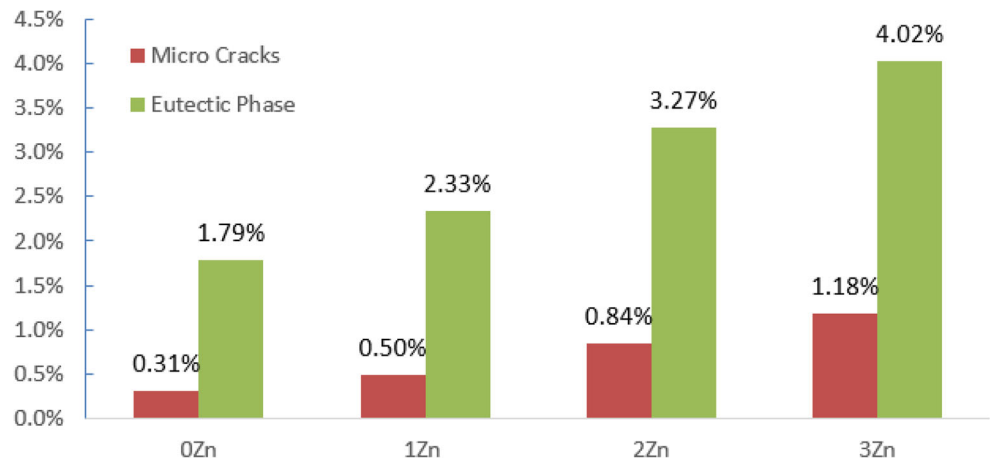

Fig. 5 SEM images from transverse sections: a Alloy0; b Alloy1; c Alloy2; d uncracked Alloy3; e morphology of micro-cracks from uncracked Alloy3 weld

Fig. 6 Percentage of pixels of microcracks and eutectic phases in the SEM image

solidification cracking index of Alloy0, Alloy1, Alloy2 specimens is 0. It implies that cracking susceptibility of all these specimens is lower than that of Alloy3 and AlloyC.

3.3 Microstructure observation

Figure 5 shows the SEM images of all welds of Alloy0, Alloy1, Alloy2, and uncracked Alloy3 welds. The microcracks always coincided with second phases. Figure 6 lists the percentages of pixels of micro-cracks and eutectic phase in the SEM image. It is found that the number of these microcracks increases with an increase of Zn content, which means solidification cracking susceptibility increases with increasing Zn content. The amount of eutectic phase also increases with an increase of Zn content. The percentage of pixel of eutectic phase shows a similar tendency with the number of microcracks. It means that the distribution density of micro-cracks increases as larger eutectic phases occur.

Figure 7 shows the SEM images of the cracked weld. The cracks grow along long and continuous eutectic phases at grain boundary in all welds. It proves that the existence of eutectic phases provides the opportunity for welds to crack. The distribution pattern of eutectic phases in different welds is also worth noticing. Eutectic phase tends to occur dispersedly in welds with lower cracking susceptibility, while long and continuous eutectic phases are always found in welds with higher cracking susceptibility. From the microstructure observation, the rank of solidification cracking susceptibility from largest to smallest among all tested alloys is as follows: AlloyC > Alloy3 > Alloy2 > Alloy1 > Alloy0.

4 Simulation and discussion

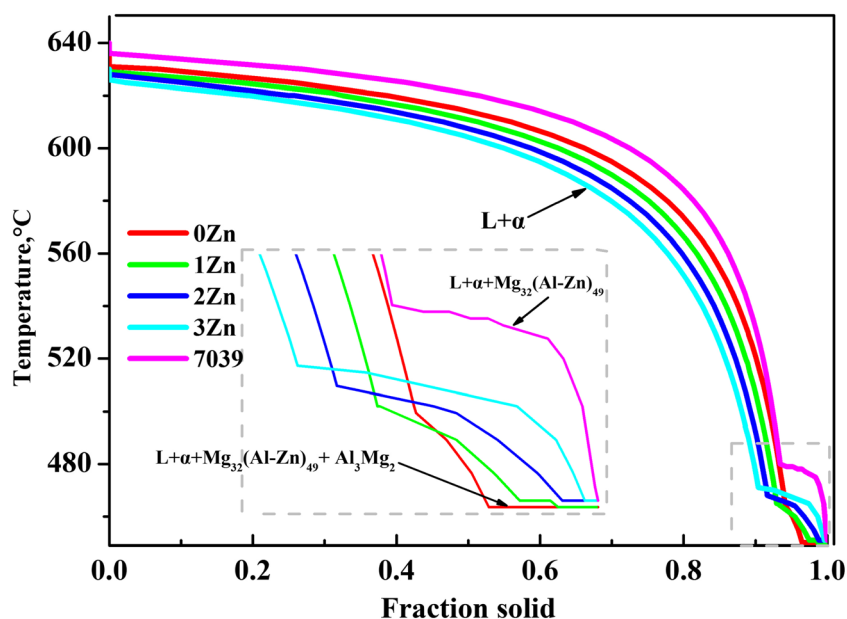### 4.1 Effect of non-equilibrium solidification behavior on the weldability

In this part, non-equilibrium solidification behavior of all alloys is calculated to find out the solidification features during welding processes. It is assumed that Mg and Zn losses due to high welding temperature are not significant enough to change the composition of alloys. The relationship between fraction solid changes and temperature decrease are studied to find out the solidification features of all tested alloys during non-equilibrium welding solidification processes. Simulations are based on the "no solid diffusion and complete liquid diffusion" model. The solidification paths and simulation result are shown in Fig. 8. Two stages of eutectic reactions take place during solidification process. $Mg_{32}(AlZn)_{49}$ is the eutectic product during stage 1 that happened between 463 and 479 °C and Al_3Mg_2 is the eutectic product during stage 2 that happened at 450 °C. It should be noted that the eutectic product of stage 1 for Alloy0 is $Mg_{32}Al_{49}$. Moreover, AlloyC has no eutectic reaction of stage 2 according to this simulation.

Table 2 shows the solidification temperature range, eutectic temperature range, fraction solid as starting eutectic reaction,
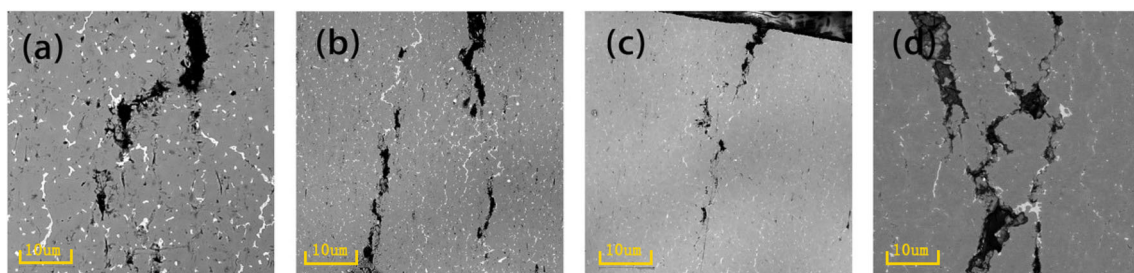
Fig. 7 Cracks growing along eutectic phase of Alloy3 **a** [direction A] and **b** [direction B] and AlloyC **c** [direction A] and **d** [direction B]

Fig. 8 The non-equilibrium so-
lidification behavior of all tested
alloys

and fraction solid as starting Al$_3$Mg$_2$ eutectic reaction during non-equilibrium solidification. The starting temperature of eutectic reaction increases with increasing Zn/Mg ratio, which is 463 °C for Alloy0, 465 °C for Alloy1, 468 °C for Alloy2, and 471 °C for Alloy3, respectively. The eutectic reaction temperature range increases with increasing Zn/Mg ratio, while the fraction solid as starting eutectic reaction decreases with increasing Zn/Mg ratio. It means that the number of eutectic phases increase with an increase of Zn/Mg ratio and corresponds to the SEM results. As for AlloyC, higher eutectic reaction starting temperature of 479 °C and wider eutectic temperature range of 29 °C are found than other alloys, but the fraction solid as starting eutectic reaction is only lower than Alloy0, which is 93.5%.
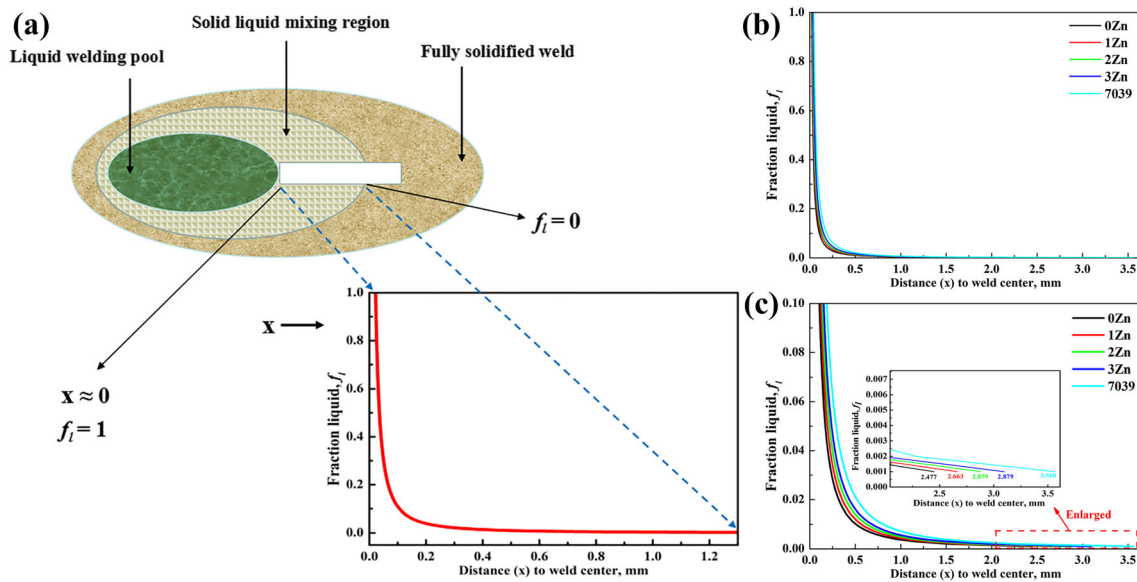
In the current study, the eutectic reaction completed at a temperature of 450 °C, where the fraction solid is higher than 99.99%. Thus, the terminal stage of solidification can be defined as the second stage Al$_3$Mg$_2$ eutectic reaction, where the fraction solid is higher than 96%. The higher amount of eutectic liquid between grains can be abundant enough to heal the incipient cracks. Thus, the solidification cracking tendency during welding increases with increasing Zn content. The fraction liquid for

AlloyC is 0. As Fig. 5 shows, the amount of eutectic phase observed in uncracked welds increases with an increase of Zn/Mg ratio. Although the weld of AlloyC has less eutectic phases than the other four welds, large-scaled eutectic phases in continuous shape can still be observed on its grain boundaries.

Wider eutectic temperature range and more eutectic phases occur with an increase of Zn/Mg ratio, providing more time for liquid eutectic phases to converge during solidification process. Simulation results also confirm that AlloyC has the widest eutectic temperature range. Thus, it can still form sizable continuous eutectic phases during solidification process even with less amount of them. The liquid eutectic phases on grain boundaries are neither able to bear nor to transfer constraining stress during solidification, and the existence of large and continuous liquid zone will bring more severe problem of stress concentration, thus leading to more serious solidification cracking phenomenon in alloys having higher Zn/Mg ratio. In the modern solidification cracking theory, not only the solidification range, the width of the mushy zone, and the feeding of continuous eutectic liquid are considered, but also the grain boundary, where cracking occurs. In the previous Scheil model, the back diffusion of elements was

Table 2   Non-equilibrium solidification behavior of tested specimens

	Solidification temperature range (°C)	Eutectic reaction temperature range (°C)	Fraction solid as starting eutectic reaction	Fraction solid as starting Al3Mg2 eutectic reaction
Alloy0	181	13	0.94	0.963
Alloy1	179	15	0.93	0.975
Alloy2	178	18	0.915	0.989
Alloy3	176	21	0.905	0.996
AlloyC	186	29	0.935	1

Fig. 9 Fraction liquid distribution as a function of distance within mushy zone: **a** schematic illustration of the mushy zone, **b** f_L as a function of x ($0 < f_L < 1$), and **c** expanded view near the terminal stage of solidification ($0 < f_L < 0.1$)

not considered. The significant back diffusion of Mg in Al-Mg alloy plays an important role in the feeding of solidification cracks [26]. Therefore, we need to consider all these factors comprehensively. The solidification range of Al-Mg-Zn in our studies is relatively lower compared with Alloy 7039. Thus, the continuous eutectic liquid feeding effects are not very significant. It is more crack susceptible in Alloy 7039, despite more continuous eutectic liquid, which is not contrary to our conclusion. The competition between all these factors on solidification cracking should be clarified in the further study.

4.2 Effect of mushy zone on the weldability

Solidification cracking susceptibility during welding not only depends primarily on the eutectic reaction temperature range and amount of liquid during terminal solidification, but also on the distribution of liquid in the solid/liquid mushy zone. Here, the authors simulate the liquid distribution pattern in the melted zone and mushy zone during solidification, as this is a more intuitive way to illustrate the fraction liquid at different places near the weld metal. A model has been developed to estimate the size of mushy zone in steels and variation of fraction liquid with distance within the mushy zone [21]. According to solidification solute redistribute laws, the temperature of liquid at any point on the liquidus line can be described as Eq. 1, assuming solidus and liquidus lines as straight lines.

$$T = T_m + \sum m_{L,i} \times C_{L,i} \qquad (1)$$

Here T refers to liquid temperature, T_m refers to the melting point of pure Al (solvent), $m_{L,i}$ is the slope of liquidus line for solute i, and $C_{L,i}$ is the liquid content for solute i. Because the diffusion patterns of solute i are close to no solid diffusion and

complete liquid diffusion, the solute redistribution of solute elements can thus be written by Scheil equation:

$$C_{L,i} = C_{0,i} f_L^{k_i-1} \qquad (2)$$

$C_{0,i}$ and k_i are the initial melt compositions of solute i, and equilibrium partition ratio of solute i, respectively. f_L refers to fraction liquid at any time. The k_i of Mg, Zn, and Cu elements are -443.2, -335.3, and -570, and $m_{L,i}$ of Mg, Zn, and Cu elements are 0.329, 0.429, and 0.12, respectively, determined in each binary phase diagram. Aiming to understand the spatial distribution pattern of fraction liquid, the distance that a point on the specimen from the weld center is set as 'x', and the temperature gradient in the mushy zone is introduced as G. To simplify modeling, G is considered as a constant, and the temperature when $x = 0$ is set to the melting point of the alloy. Based on this model, temperature in the mushy zone at any distance can be found as

$$T = T_L - Gx \qquad (3)$$

By combining above equations, how f_L changes with x in the mushy zone is finally determined by Eq. 4.

$$T_L - Gx = T_m + m_{L,i} C_{0,i} f_L^{k_i-1} \qquad (4)$$

The fraction liquid as a function of distance in the mushy zone can be illustrated in Fig. 9. As the distance to the centerline of a weld increases, fraction liquid drops dramatically, and this trend gets slow as it goes deeper in the mushy zone. It is obvious that AlloyC has the widest mushy zone, followed by Alloy3, Alloy2, Alloy1, Alloy0. It means that under the same cooling condition, the time needed for solidification increases with increasing Zn/Mg ratio. This is mainly due to their decreasing eutectic

temperature range, and this result is exactly in line with the solidification behavior simulated in section 4.1. As a result, the solidification cracking tendency during welding of 7039 Al alloys is higher than the current studied alloys.

5 Conclusions

This paper systematically investigates the solidification cracking behavior of Al-Mg-Zn alloy with a Zn/Mg ratio below 1.0 during welding process and compared with alloy 7039 with a Zn/Mg ratio above 1.0. The main points are concluded as follows:

(1) The tensile strength of the novel alloy increases with an increase of Zn content and is higher than Alloy 7039. The solidification cracking susceptibility of the developed Al-Mg-Zn alloy is lower than a common 7xxx alloy, Alloy 7039. The solidification cracking susceptibility increases with increasing Zn content.

(2) Increase in the Zn/Mg ratio will result into higher eutectic proportion, wider eutectic temperature range, and wider mushy zone in the alloy systems and thus increase the chances for the occurrence of large and continuous liquid eutectic phase.

Compliance with ethical standards

References

1. Dursun T, Soutis C (2014) Recent developments in advanced aircraft aluminium alloys. Mater Des 56:862–871
2. Azarniya A, Taheri AK, Taheri KK (2019) Recent advances in ageing of 7xxx series aluminum alloys: a physical metallurgy perspective. J Alloys Compd 781:945–983
3. Liptak JA, Baysinger FR (1968) Welding dissimilar aluminum alloys. Weld J 47:173s–180s
4. McMahon ME, Harris ZD, Scully JR, Burns JT (2019) The effect of electrode potential on stress corrosion cracking in highly sensitized Al-Mg alloys. Mater Sci Eng A 767:138399
5. Seifi M, Ghamarian I, Samimi P, Collins C, Holroyd NJH, Lewandowski JJ (2018) Sensitization and remediation effects on environmentally assisted cracking of Al-Mg naval alloys. Corros Sci 138:219–241
6. Srinivasa Rao K, Prasad Rao K (2005) Partially melted zone in Al-Mg-Si alloy gas tungsten arc welds: effect of techniques and prior thermal temper. Mater Sci Technol 21:995–1002
7. Beiranvand ZM, Ghaini FM, Moosavy HN, Sheikhi M, Torkamany MJ (2019) Solidification cracking susceptibility in pulsed laser welding of Al-Mg alloys. Materialia 7:100417
8. Kou S, Le Y (1985) Grain structure and solidification cracking in oscillated arc welds of 5052 aluminium alloy. Metall Trans A 16A: 1345–1352
9. Chua SF, Chen HC, Bi G (2019) Influence of pulse energy density in micro laser weld of crack sensitive Al alloy sheets. J Manufac Proc 38: 1–8
10. Zhou Y, Qin R, Xiao S, He G, Zhou B (2000) Reversing effect of electropulsing on damage of 1045 steel. J Mater Res 15:1056–1061
11. Qbau N, Nam ND, Ca NX, Hien NT (2020) The crack healing effect of scandium in aluminum alloys during laser additive manufacturing. J Manufac Proc 50:241–246
12. Cross CE, Grong O (1998) Microstructure and mechanical properties of simulated Al-Mg-Zn weld metal modified with Sc and Zr. Proc. 6th international Conference on Aluminum Alloys (ICAA-6), Toyohashi 3:1441–1446
13. Yang F, Liu E, Xu J, Zhang Z, Shi L (2010) Hot cracking susceptibility of (Sc, Zr, Er) microalloyed Al-5Mg filler metals. The Chinese J Nonferrous Metals 20:620–627
14. Mukhopadhyay AK, Reddy GM (2002) Influence of trace addition of Ag on the weldability of Al-Zn-Mg-Cu-Zr base 7010 alloy. Mater Sci Forum 396-402:1665–1670
15. Mukhopadhyay AK, Prasak KS, Kumar V (2006) Key microstructural features responsible for improved stress corrosion cracking resistance and weldability in 7xxx series Al alloys containing micro/trace alloying additions. Mater Sci Forum 519-521:315–320
16. Guan R, Shen Y, Zhao Z, Wang X (2017) A high-strength, ductile Al-0.35Sc-0.2Zr alloy with good electrical conductivity strengthened by coherent nanosized-precipitates. J Mater Sci Technol 33:215–223
17. He L, Cao Y, Zhou Y, Cui J (2018) Effects of Ag addition on the microstructures and properties of Al–Mg–Si–Cu alloys. Int J Min Met Mater 25:62–72
18. Bai S, Huang T, Xu H, Liu Z, Wang J, Yi X (2019) Effects of small Er addition on the microstructural evolution and strength properties of an Al–Cu–Mg–Ag alloy aged at 200° C. Mater Sci Eng A 766:138351
19. Ram GJ, Mitra TK, Raju MK, Sundaresan S (2000) Use of inoculants to refine weld solidification structure and improve weldability in type 2090 Al-Li alloy. Mater Sci Eng A 276:48–57
20. DuPont JN, Notis MR, Marder AR (1998) Solidification of Nb-bearing superalloys: part 1. Reaction sequences. Metall Mater Trans A 29A:2785–2796
21. DuPont JN, Robino CV, Marder AR (1999) Modelling mushy zones in welds of multicomponent alloys: implications for solidification cracking. Sci Technol Weld Join 4:1–14
22. Soysal T, Kou S (2018) A simple test for assessing solidification cracking susceptibility and checking validity of susceptibility prediction. Acta Mater 143:181–197
23. Hou SL, Liu PP, Zhang D, Zhang JS, Zhuang LZ (2018) Precipitation hardening behavior and microstructure evolution of Al-5.1Mg-0.15Cu alloy with 3.0Zn. J Mater Sci 53:3846–3861
24. Hou SL, Zhang D, Ding QW, Zhuang LZ, Zhang JS (2019) Solute clustering and precipitation of Al-5.1Mg-0.15Cu-xZn alloy. Mater Sci Eng A 759:465–478
25. Ding QW, Zhang D, Pan YL, Hou SL, Zhuang LZ, Zhang JS (2019) Strengthening mechanism of age-hardenable Al-x-mg-3Zn alloys. Mater Sci Tech 35:1071–1080
26. Liu J, Duarte HP, Kou S (2017) Evidence of back diffusion reducing cracking during solidification. Acta Mater 122:47–59